Catalysis Today 143 (2009) 38–44

Contents lists available at ScienceDirect

Catalysis Today

journal homepage: www.elsevier.com/locate/cattod

Cobalt oxide supported on alumina catalysts prepared by various methods for use in catalytic afterburner of PEM fuel cell

I. Zacharaki [a,d], C.G. Kontoyannis [b,d], S. Boghosian [c,d], A. Lycourghiotis [a], Ch. Kordulis [a,d,*]

[a] Department of Chemistry, University of Patras, GR-26500 Patras, Greece
[b] Department of Pharmacy, University of Patras, GR-26500 Patras, Greece
[c] Department of Chemical Engineering, University of Patras, GR-26500 Patras, Greece
[d] Institute of Chemical Engineering and High Temperature Chemical Processes (FORTH/ICE-HT), GR-26500 Patras, Greece

ARTICLE INFO

Article history:
Available online 7 November 2008

Keywords:
Cobalt oxide catalysts
Combustion catalysts
Afterburner
PEM fuel cell
EDF
Catalyst preparation
Energy
Methane oxidation
Methanation

ABSTRACT

In the present work we have investigated the influence of the preparation method on the physicochemical and activity features of CoO_x/γ-Al_2O_3 catalysts used for the combustion of anode tail gas produced in a proton-exchange membrane (PEM) fuel cell. The catalysts prepared contain 21% (w/w) Co and have been calcined at 850 °C. Three different impregnation methodologies have been followed: incipient wetness impregnation (IWI) using a cobalt nitrate aqueous solution, incipient wetness impregnation using a mixed cobalt nitrate–nitrilotriacetic acid (IWI-nta) aqueous solution and equilibrium deposition filtration (EDF) using a cobalt nitrate aqueous solution. The catalysts were characterized using nitrogen adsorption for determining the specific surface area, the pore volume and the mean pore diameter as well as using X-ray powder diffraction (XRD), diffuse reflectance spectroscopy (DRS; UV–vis), LRS, X-ray photoelectron spectroscopy (XPS) and temperature-programmed reduction (TPR). Catalytic activity measurements were performed in the temperature range 250–850 °C using a continuous flow fixed-bed micro-reactor working under atmospheric pressure and fed with a reaction mixture consisted of 15% H_2/3% CO/1.1% CH_4/20% O_2 balanced in He.

The EDF methodology imposed interfacial deposition and resulted to the formation of an almost bi-dimensional surface precipitate. Upon calcination, this surface precipitate provided a very well-dispersed CoO_x amorphous species strongly interacted with the support surface and thus hardly reducible as well as relatively small Co_3O_4 supported nanocrystals (14.3 nm). The first phase is the predominant one. Therefore, EDF resulted to a catalyst with the highest cobalt surface and specific surface area. The conventional IWI imposed bulk (solution) precipitation and thus induced relatively large supported crystallites which upon calcination provided relatively large supported Co_3O_4 nanocrystals (19.8 nm) and $CoAl_2O_4$ as well. The formation of the relatively large nanocrystals and the insertion of cobalt inside the γ-alumina lattice to form $CoAl_2O_4$ may be responsible for the lowest cobalt surface obtained in this catalyst. The presence of the nitrilotriacetic acid in the impregnating solution induced the exchange of the water ligands of the Co(II) aqua complex present in the cobalt nitrate solution with organic ligands and thus the bulk precipitation of an organometallic complex. The more bulky organic ligands decreased the cobalt-support interactions. Thus, the insertion of cobalt inside the γ-alumina lattice and the formation of $CoAl_2O_4$ are inhibited upon calcination of the IWI-nta sample. This may be responsible for the relatively higher cobalt surface obtained with respect to that achieved in the IWI sample though the size of the Co_3O_4 nanocrystals is larger in the IWI-nta sample (25.8 nm). At relatively high reaction temperatures all catalysts exhibited almost the same activity for oxidation reactions. In contrast, at low reaction temperatures the EDF catalyst proved to be more active for the CH_4 production as well as for the oxidation of H_2 and CO. This behaviour may be attributed to the favourable physicochemical characteristics of this catalyst.

* Corresponding author at: Department of Chemistry, University of Patras, University campus, GR-26500 Patras, Greece. Tel.: +30 2610 997 125; fax: +30 2610 994 796.
E-mail address: kordulis@chemistry.upatras.gr (C. Kordulis).

0920-5861/$ – see front matter © 2008 Elsevier B.V. All rights reserved.
doi:10.1016/j.cattod.2008.09.026

1. Introduction

The rapid development in recent years of the proton-exchange membrane (PEM) fuel cell technology has stimulated research in all areas of catalysts used for generation of pure hydrogen (fuel reforming, water–gas shift and carbon monoxide preferential oxidation) as well as of anode tail gas combustion catalysts [1,2]. The principal aim in the latter case is the efficient use of the fuel cell effluents (CO, H_2 and CH_4) to produce via oxidation reactions the energy necessary for the hydrogen generation reactors and to minimize the CH_4 and CO emissions. Catalytic or non-catalytic burners are generally used for this purpose [2]. It should be noted that CH_4 is much more powerful greenhouse gas than CO_2.

Among the components of the effluent of a fuel cell, hydrogen is the most easily combusted. The opposite is true for the complete oxidation of any CH_4 present. Methane is, in effect, the least reactive of the hydrocarbons and therefore the most difficult to oxidise. It has been found that conventional three-way catalysts (containing Pd–Pt–Rh), currently used for gasoline-vehicle emissions control, show relatively poor methane conversion, when operating in stoichiometric air/fuel ratio [3]. In contrast, Pd–Pt catalysts are quite effective for methane oxidation [4]. On this basis, new catalysts containing Pd or Pd–Pt have to be designed in order to replace the conventional Pd–Pt–Rh catalysts [5]. Thus, a lot of research effort is addressed to this subject [6–13]. On the other hand, current commercial catalysts for cleaning exhausts from *natural gas vehicles* have three times higher noble metals (Pd–Pt) content (up to 300 g/ft^3) than the standard gasoline three-way catalysts in order to oxidise methane efficiently [14].

Considering the relevant cost of precious metals the design of alternative and cheaper systems would be highly desirable [5]. Non-precious metal catalysts supported on various carriers seem to be a good alternative, especially for feeds without sulfur, as in the case of PEM fuel cell [15–22]. Cobalt oxide supported, mainly, on alumina as well as on other oxide supports is one of the most popular candidates studied for methane combustion [21–24]. The supported species formed on the surface of these catalysts, their dispersion and the strength of their interaction with the support as well as the nature of the latter influence drastically the activity of the above-mentioned catalysts.

We have recently studied cobalt oxide catalysts supported on γ-alumina [25–28]. It has been found that the preparation method followed has remarkable influence on the structural and activity features of these catalysts. A relatively large size of the supported "cobalt oxide" nanocrystallites is imposed by *bulk precipitation*. This is mainly realized by incipient wetness impregnation (IWI). In contrast, a quite small size of the supported "cobalt oxide" nanocrystallites, not strongly interacted with the support surface, is imposed by *interfacial precipitation*. This is realized by equilibrium deposition filtration (EDF) [29,30]. This phase has been found to be the optimum supported phase for complete oxidation reactions (e.g. benzene oxidation) [30].

In the above-mentioned studies [25–30] the calcination temperature did not exceed 650 °C. On the other hand in an "afterburner" the temperature reaches, and in some cases exceeds, 800 °C. For this reason in the present work we have investigated the influence of preparation method on activity features of CoO_x/γ-Al_2O_3 catalysts *calcined at 850 °C*. Specifically, we have compared the catalytic activity of three "cobalt oxide"/γ-alumina catalysts prepared by three different preparation methodologies: conventional IWI using a cobalt nitrate aqueous solution, incipient wetness impregnation using a mixed cobalt nitrate–nitrilotriacetic acid aqueous solution (IWI-nta) [31] and EDF using a cobalt nitrate aqueous solution [32–36].

The second, *also principal*, goal of the present work is to examine whether the change in the impregnation method could influence the final physicochemical characteristics of cobalt-supported γ-alumina catalysts calcined at relatively high temperature (850 °C). This will allow interpreting eventual differences in the catalytic activity by taking into account the changes in the physicochemical characteristics of the supported catalysts brought about by replacing the conventional IWI technique with the aforementioned impregnation methods. Thus, the catalysts prepared have been characterized using, jointly, various physicochemical techniques (BET, XRD, UV–vis DRS, XPS, Raman and TPR).

2. Experimental

2.1. Preparation of the catalysts

2.1.1. Materials

Cobalt nitrate hexahydrate [$Co(NO_3)\cdot 6H_2O$, 99% of purity] purchased from Merck has been used for the preparation of the solutions used in the preparation of the catalysts. Ammonium nitrate stock solutions, used for regulating the ionic strength, were prepared from the respective solid (Merck, 99% of purity). Nitrilotriacetic acid 2 M solution was used in the preparation of the IWI-nta catalyst. γ-Alumina powder, 90–150 μm, was used as support. This is obtained by crushing AKZO γ-alumina extrudates (HDS-000-1.5mm E).

2.1.2. Preparation of the IWI sample

The IWI sample was prepared using successive dry impregnations of the support with suitable $Co(NO_3)_2$ aqueous solutions in order to obtain a final catalyst containing 21% (w/w) Co. After each impregnation step the sample was dried at 120 °C for 2.5 h and the final sample was calcined at 850 °C for 3 h.

2.1.3. Preparation of the IWI-nta sample

The IWI-nta sample, containing also 21% (w/w) Co, was prepared using successive dry impregnations. The solutions used in the impregnations were prepared by dissolving a given amount of the $Co(NO_3)_2\cdot 6H_2O$ in an aqueous solution of nitrilotriacetic acid 2 M. The pH of this solution was regulated to be equal to seven. The impregnated material had a gel-like appearance and after drying at 120 °C for 2.5 h was transformed into a hard solid. The latter was crushed before the next impregnation. The final sample was calcined at 850 °C for 3 h.

2.1.4. Preparation of the EDF sample

The EDF sample was prepared at 25.0 ± 0.1 °C and pH 7.0 under N_2 atmosphere. A thermostated vessel (10 L) equipped with a pH control system involving a glass/saturated calomel electrode (Metrhom) and a dosimat has been used. A volume of 5.0 L of cobalt nitrate solution (25×10^{-3} M) was purred in this vessel and its ionic strength was adjusted at 0.1 M by using NH_4NO_3. The pH was adjusted by adding NH_4OH 0.1 M aqueous solution under stirring. Ten grams of γ-alumina powder was added into the stirred solution. As the deposition of the $Co(H_2O)_6^{2+}$ ions onto the alumina surface caused a decrease in the pH of the suspension, the pH control system fed a suitable amount of the NH_4OH solution to keep pH 7. When the pH control system stopped to feed NH_4OH solution, the suspension was filtered. The solid sample was dried in air at 120 °C for 2.5 h and calcined at 850 °C for 3 h. The Co(II) concentration in the solid was 21% (w/w). This was determined by measuring photometrically its concentration in the corresponding impregnating solution before and after deposition using a Cary 3 Varian spectrophotometer. The above measurements were based on the Nitroso R-Salz procedure [37].

2.2. Characterization of the catalysts

2.2.1. Specific surface area (SSA)

The physical adsorption–desorption isotherms of N_2 at −196 °C were obtained on a Micromeritics TriStar 3000 instrument. Around 100–200 mg of sample was used, previously degassed at 250 °C for 1 h. The data were processed using software from Micromeritics Corporation. The SSAs were calculated from data acquired in the relative pressure (P/P_0) range of 0.01–0.30.

2.2.2. X-ray powder diffraction

XRD patterns of the catalysts were obtained with a Bruker D8—advanced diffractometer by using Ni-filtered Cu Kα radiation (λ = 0.15418 nm). The generator is equipped with a sensitive detector PSD Lynxey operated at 40 kV and 40 mA. The samples in powder form were analyzed without a previous treatment after deposition on a stainless steel sample holder. The XRD data were collected in 2θ range 25–70°, the scan speed and step size being 0.3° min^{-1} and 0.02°, respectively. Mean crystallite size ($d_{cryst.}$) of the Co-phase was calculated from the line broadening using the well-known Scherrer equation [21].

2.2.3. Diffuse reflectance spectroscopy

The diffuse reflectance spectra of the samples studied were recorded in the range 200–800 nm at room temperature after calcination, using a UV–vis spectrophotometer (Varian Cary 3) equipped with an integration sphere. The γ-Al_2O_3 carrier was used as a reference in all cases and for diluting the calcined samples which exhibited extremely high absorbance. The powder samples were mounted in a quartz cell which provided a sample thickness greater than 3 mm and thus guaranteed "infinite" sample thickness.

2.2.4. Raman spectroscopy

The kinds of the Co species formed on the surface of the γ-alumina support for the catalyst samples prepared following the three different preparation methods were studied by *in situ* Raman spectroscopy. Approximately 90 mg of each catalyst in powder form were pressed into a wafer and mounted on a holder that could be adjusted in the vertical core of the *in situ* Raman cell, which is described elsewhere [38]. The 514.5 nm line of a Spectra Physics Stabilite 2017 Ar^+ laser operated at 30 mW on the sample was used for recording the Raman spectra. The laser beam was focused on the sample with a cylindrical lens in order to reduce sample irradiance. The scattered light was collected at 90°, analyzed with a 0.85 m Spex 1403 double monochromator and detected by a −20 °C cooled RCA PMT equipped with EG&G photon counting electronics. Recording of spectra started at 300 °C under flowing O_2 after the sample was exposed for 1 h at 300 °C in flowing O_2. Subsequently, spectra were recorded after cooling the furnace to 25 °C under O_2 and at 300 °C under a flowing 4.5% H_2/N_2 mixture. Finally, the sample was re-oxidised at 300 °C and the reinstatement of the surface composition was confirmed by reproducing the Raman spectra under oxidised conditions.

2.2.5. X-ray photoelectron spectroscopy

The XPS analysis of the calcined samples was performed at room temperature in an UHV chamber (base pressure 8×10^{-10} mbar) which consists of a fast specimen entry assembly, a preparation and an analysis chamber. The residual pressure in the analysis chamber was below 10^{-8} mbar. The latter was equipped with a hemispherical electron energy analyzer (SPECS, LH 10) and a twin-anode X-ray gun for XPS. The unmonochromatized Mg Kα line at 1253.6 eV and a constant pass energy mode for the analyzer were used in the experiments. Pass energies of 36 and 97 eV resulted at a full width at half-maximum (fwhm) of 0.9 and 1.6 eV, respectively, for the Ag $3d_{5/2}$ peak of a reference foil. The binding energies were calculated with respect to the C 1 s peak (C–C and C–H) set at 284.6 eV. The normalized intensities I_{Co2p}, I_{A12p} and I_{O1s} of the corresponding XPS peaks, corrected using the sensitivity factors published by Wagner et al. [39], were used to determine the atomic surface composition of the catalysts studied.

2.2.6. Temperature-programmed reduction

The TPR experiments were performed in laboratory-constructed equipment described elsewhere [40] in which the ideas of the Rogers–Amenomiya–Robertson arrangement have been followed [41]. An amount of sample (0.1 g) was placed in a quartz reactor and the reducing gas mixture (H_2/Ar:5/95, v/v) was passed through it for 2 h with a flow rate of 40 mL min^{-1} at room temperature. Then the temperature was increased to 900 °C with a constant rate of 10 °C min^{-1}. Reduction leads to a decrease of the hydrogen concentration in the gas mixture, which was detected by a thermal conductivity detector (TCD). The reducing gas mixture was dried in a cold trap (−95 °C) before reaching the TCD.

2.2.7. Catalytic activity measurements

Catalytic activity measurements were performed in a continuous flow fixed-bed micro-reactor working under atmospheric pressure. The reaction mixture consisted of 15% H_2/3% CO/1.1% CH_4/20% O_2 balanced in He. Specimens of 100 mg of non-diluted catalyst (catalytic bed 1 cm in height and 0.35 cm in diameter) were used in these measurements. The reaction mixture was fed in the reactor with a flow rate of 200 mL min^{-1} (STP) and the catalytic tests were carried out in the temperature range 250–850 °C. Reagents and products were analyzed by a gas chromatograph (Shimadzu, GC-14B) equipped with a TCD and a capillary column (Carboxen 1000).

3. Results and discussion

3.1. Catalytic activity

Fig. 1 shows the CH_4 conversion obtained at various reaction temperatures over the three prepared catalysts as well as over the γ-alumina used as catalytic support. This figure indicates the function of two antagonistic reactions: methanation (1) which provides negative values for conversion and oxidation of methane

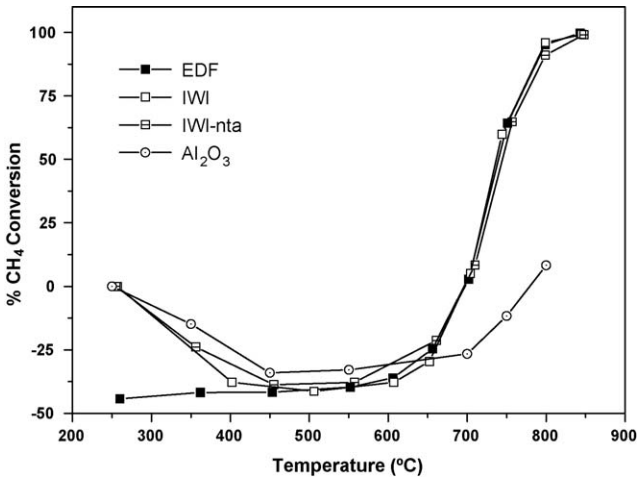

Fig. 1. Methane conversion over the CoO_x/Al_2O_3 catalysts and the Al_2O_3 used as support.

(2) providing positive conversion values:

$$CO + 3H_2 \rightarrow CH_4 + H_2O \quad (1)$$

$$CH_4 + 2O_2 \rightarrow CO_2 + H_2O \quad (2)$$

The first reaction predominates in the temperature range 250–700 °C whereas the second at temperatures higher than 750 °C. It may be seen that pure alumina exhibited relatively low activity for the CH_4 combustion under our experimental conditions. In contrast, the supported CoO_x species proved to be quite active for this reaction. It may be, moreover, seen that CH_4 formation was also higher over the CoO_x/Al_2O_3 catalysts than that over γ-alumina. The studied CoO_x/Al_2O_3 catalysts exhibited the same catalytic behaviour at reaction temperatures higher than 450 °C. Below this temperature the EDF catalyst was proved to be the most active for methanation reaction. In fact, a significant amount of CH_4 was formed over this sample even at the lowest reaction temperature studied.

Fig. 2 illustrates the hydrogen conversion achieved over the catalysts prepared and the support at reaction temperatures in the range 250–850 °C. Hydrogen is consumed in both oxidation (3) and methanation (1) reactions:

$$H_2 + 1/2O_2 \rightarrow H_2O \quad (3)$$

This is the reason for which we observe a monotonous increase of the hydrogen conversion with temperature (Fig. 2). From Figs. 1 and 2, it may be inferred that at relatively low (high) temperatures hydrogen is mainly consumed in methanation (oxidation) reaction. The most important observation concerning Fig. 2 is the complete hydrogen consumption over the EDF catalyst even at the lowest reaction temperature. This should be related to the aforementioned very high methanation activity of this catalyst. At relatively low reaction temperatures ($T < 450$ °C) the activity of the rest catalytic samples is lower than that of the EDF sample and almost the same to that of the support. However, alumina proved to be very active for H_2 consuming reactions at high reaction temperatures ($T \geq 450$ °C).

Fig. 3 illustrates the CO conversion as a function of temperature over the CoO_x/Al_2O_3 catalysts and the support. Carbon monoxide is also consumed in both oxidation (4) and methanation (1) reactions:

$$CO + 1/2O_2 \rightarrow CO_2 \quad (4)$$

Therefore, a monotonous increase of the CO conversion with temperature is expectable. From Fig. 3, it emerges that the EDF

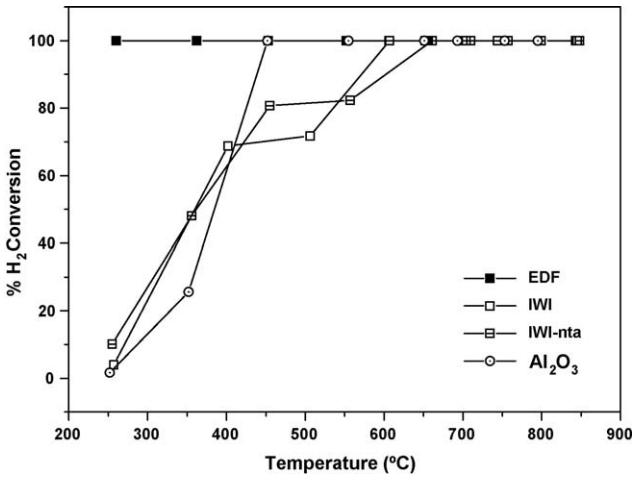

Fig. 2. Hydrogen conversion over the CoO_x/Al_2O_3 catalysts and the γ-alumina used as support.

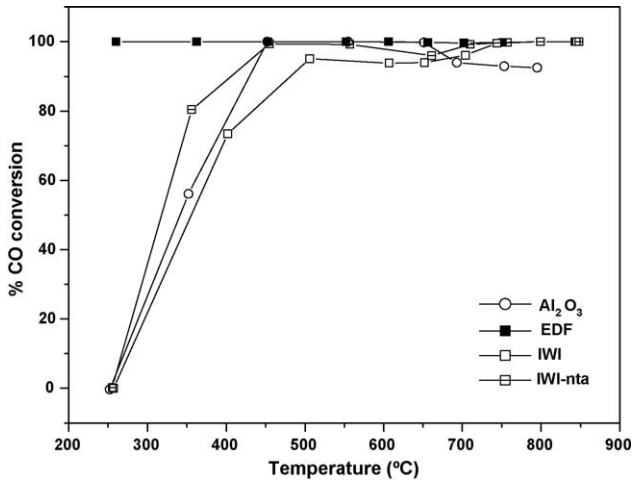

Fig. 3. Carbon monoxide conversion over the CoO_x/Al_2O_3 catalysts and γ-alumina used as support.

sample exhibits the highest activity for the CO consuming reactions as complete CO conversion is achieved *only over this sample at reaction temperatures lower than 450 °C*. The corresponding catalytic behaviour of the rest CoO_x/Al_2O_3 catalysts seems to be similar to that of the support.

Let us now examine whether the reactions taking place in the temperature range 250–450 °C involve exclusively methanation or both methanation and oxidation. The highest CH_4 production has been observed over the EDF catalyst at 250 °C. This production corresponds to H_2 and CO conversions equal to 10 and 17%, respectively. However, as it may be seen from Figs. 2 and 3, the corresponding experimental conversions obtained over this catalyst at the same temperature were in both of cases equal to 100%. This means that reactions (3) and (4), and probably (2) are also accelerated over this catalyst. The same conclusion can be also drawn concerning the catalytic behaviour of all catalysts and the support in the temperature range 250–450 °C. The above deductive reasoning was inevitable in our case, since the direct measurement of the catalytic activity towards H_2 and CO oxidation was inaccurate due to incomplete resolution of the chromatographic peaks corresponding to H_2O and CO_2 produced.

3.2. Catalysts characterization

In Table 1 are compiled the textural characteristics of the catalysts prepared (BET surface area: S_{BET}, pore volume: PV, and mean pore diameter: d_p). As it can be seen from the corresponding values, the EDF sample exhibited relatively high S_{BET} and PV as well as relatively low d_p. This finding indicates indirectly that the relatively high dispersion of the supported cobalt phase achieved following the EDF methodology for the deposition of the Co(II) species on the alumina surface [25–30] is rather conserved even

Table 1
BET surface area (S_{BET}), pore volume (PV), mean pore diameter (d_p), mean crystal diameter of Co-phase ($d_{cryst.}$) and Co atomic surface concentration (% $Co_{surf.\ atoms}$) of the catalysts studied.

Catalyst	S_{BET} ($m^2\ g^{-1}$)	PV ($cm^3\ g^{-1}$)	d_p (Å)	$d_{cryst.}$(Å)[a]	% $Co_{surf.\ atoms}$[b]
IWI	111	0.42	136	198	5.4
IWI-nta	111	0.42	144	258	9.1
EDF	122	0.44	131	143	11.9

[a] Calculated from XRD patterns using the Scherrer equation.
[b] Calculated using the XPS spectra.

after *the high temperature (850 °C) calcination applied on the catalysts studied in this work.*

The XRD patterns for the catalysts studied are illustrated in Fig. 4. In these patterns relatively intensive diffraction peaks at about 31.5°, 37°, 45°, 56°, 59° and 65° which could be assigned to spinel structures of the Co_3O_4 and/or $CoAl_2O_4$ phases [23,42,43] are present in addition to several weak peaks (at about 37.5°, 46° and 67°) attributed to the support [43]. It is difficult to discriminate these cobalt phases because their diffraction patterns are very similar. On the other hand, the presence of a very well-dispersed CoO phase could not be excluded due to the absence of the corresponding peaks in the XRD patterns (see laser Raman results below).

As the most intensive XRD peak of the Co-phases (at 2θ: 37°) is overlapped with one peak assigned to the γ-alumina, we used the peak at $2\theta = 31.5°$ to calculate the mean diameter ($d_{cryst.}$) of the spinel structure Co-phases. The calculated values (Table 1) show that the highest dispersion (lowest crystal size) of these phases has been achieved in the EDF sample. This finding confirms the conclusion drawn previously on the base of the textural characteristics of the catalysts studied.

In order to investigate further the structural characteristics of the catalysts prepared we have recorded their UV–vis diffuse reflectance spectra in the region 200–800 nm (Fig. 5). All spectra exhibit an intense and not well-resolved triple absorption band, centered at around 600 nm. Two shoulders also appear: one at the low (~430 nm) and another one at the high (~720 nm) wavelength side.

The triple band is attributed to $CoAl_2O_4$ which contains Co(II) in tetrahedral symmetry [44,45]. It consists of two bands at 580 and 630 nm, and one shoulder at 545 nm. This multiple absorption can safely be assigned to the ligand-field $^4A_2 \rightarrow {}^4T_1(P)$ transition [46–48]. The two shoulders decorating the triple band are attributed to Co_3O_4 phase and they are assigned to $^1A_{1g} \rightarrow {}^1T_{1g}$ (720 nm) and $^1A_{1g} \rightarrow {}^1T_{2g}$ (430 nm) transitions [48]. Thus, the aforementioned DRS results confirm the existence of both spinel structure phases (Co_3O_4 and $CoAl_2O_4$) detected by the XRD analysis in all the catalysts studied. However, even by applying this technique it is not possible to detect any significant structural difference among the studied catalysts explaining their activity differences observed at low reaction temperatures.

Thus, in order to obtain a more clear picture about the structural characteristics of the catalysts prepared we recorded the laser Raman spectra of the samples under various atmospheres. More precisely, the Raman spectrum was recorded for each catalyst

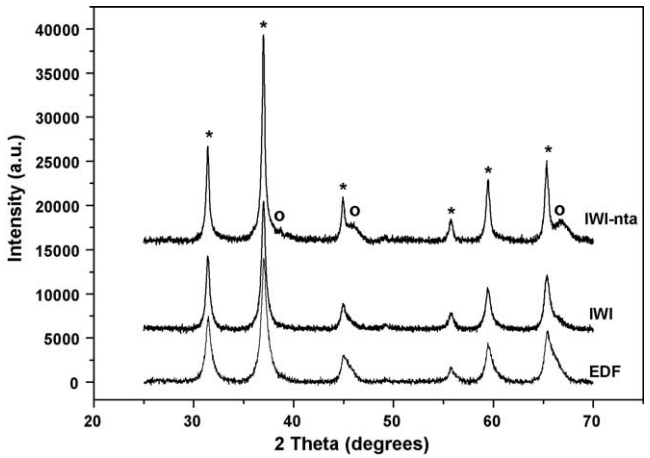

Fig. 4. XRD patterns of the CoO_x/Al_2O_3 catalysts: (*) Co_3O_4 and/or $CoAl_2O_4$; (○) Al_2O_3.

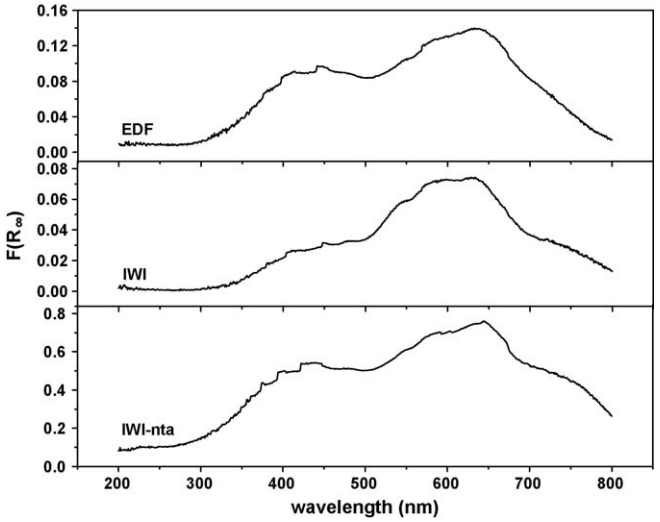

Fig. 5. UV–vis diffuse reflectance spectra of the CoO_x/Al_2O_3 catalysts.

sample at 300 °C under oxygen atmosphere. The sample was then cooled in the Raman furnace under flowing O_2 and the spectrum was recorded at room temperature. Afterwards, the Raman spectrum was recorded at 300 °C under 4.5% H_2/N_2. Finally, the sample was re-oxidised and the Raman spectrum was again recorded. The same procedure was followed for all three samples.

Fig. 6 shows the Raman spectra obtained for the catalyst samples at 25 °C. The spectra obtained at 300 °C under flowing O_2 were qualitatively the same with the respective spectra shown in Fig. 6 but the observed bands are sharper and better resolved at room temperature. Treatment with hydrogen at 300 °C did not

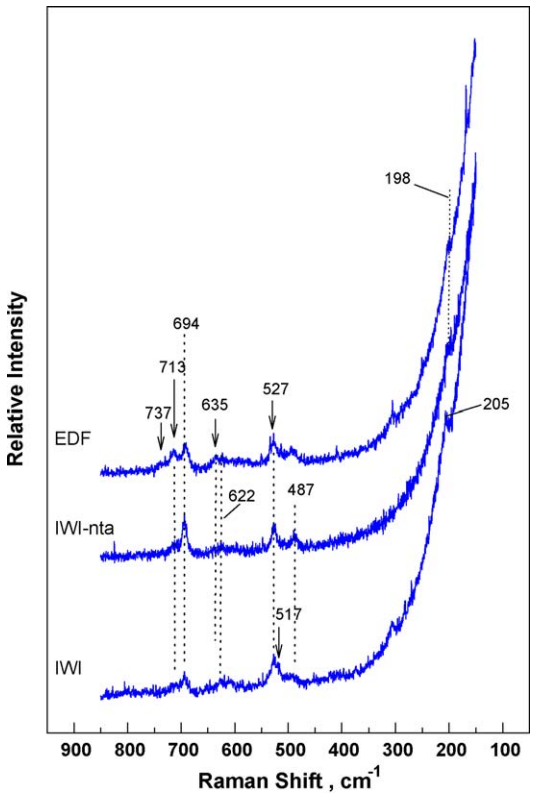

Fig. 6. Raman spectra of the CoO_x/Al_2O_3 catalysts obtained at room temperature after treatment with flowing O_2 at 300 °C. Resolution: 7 cm^{-1}.

affect the vibrational properties of the surface species, indicating that the samples are not reduced by H_2 containing gas (4.5% H_2/N_2) at this temperature, in agreement with the H_2-TPR curves, discussed below. Therefore, the discussion on surface composition and structural properties of the dispersed species will be based, for brevity, on the spectral features exhibited in Fig. 6.

The γ-Al_2O_3 is a poor Raman scatterer, therefore all bands observed in Fig. 6 are due to surface cobalt oxide species. The five characteristic bands due to the crystalline Co_3O_4 spinel with Co^{2+} and Co^{3+} located at tetrahedral and octahedral sites, respectively, dominate the spectrum of the IWI-nta sample and are identified as 694 cm^{-1} (A_{1g}), 622 cm^{-1} (F_{2g}), 527 cm^{-1} (F_{2g}), 487 cm^{-1} (E_g) and 198 cm^{-1} (F_{2g}). The observed band positions and relative intensities are in agreement with the Raman spectra of Co_3O_4 single crystals [49]. The possible occurrence of CoO phase cannot be excluded because the 484 and 691 cm^{-1} CoO bands [50] coincide with respective Co_3O_4 bands and furthermore due to a possible laser-induced conversion of CoO to Co_3O_4 [50]. The spectrum of the EDF sample exhibits also the five Co_3O_4 bands (although slightly broadened) plus at least three features at 635, 713 and 737 cm^{-1} that are not due to any of the possibly expected Co containing crystalline species (Co_3O_4, CoO and $CoAl_2O_4$) and are assigned to dispersed amorphous CoO_x species. Formation of anchoring Co–O–Al bridges can result in weakening of Co–O bonds within CoO_6 and CoO_4 units and in a corresponding strengthening (and blue shift) of non-bridging Co–O bonds protruding from the surface, thereby explaining the appearance of bands at 713 and 737 cm^{-1}. The band at 635 cm^{-1} can be due to Co–O–Co stretches of the dispersed CoO_x phase, in analogy with the relative band positions due to M–O and M–O–M modes of dispersed surface metal oxides. The broad nature of the Co_3O_4 spinel bands in spectrum of the EDF sample *is indicative of a much smaller Co_3O_4 crystal size on the surface of this sample*. Furthermore, since the scattering cross-section is generally much lower in dispersed metal oxides than in the corresponding crystalline oxides, *it appears that a significant part of the surface is composed of dispersed CoO_x*. Now, a closer inspection of the spectrum of IWI-nta sample reveals that the 713 and 635 cm^{-1} bands that we have assigned to amorphous CoO_x are also present in the spectrum of the latter sample, indicating that the amorphous phase is present to some extent also at the surface of this sample.

The Raman spectrum of the IWI sample possesses bands due to Co_3O_4 exhibiting weak and broad characteristics that are indicative of small crystal size. Additionally, bands due to $CoAl_2O_4$ at 205, ~410 and 517 cm^{-1} [42,51] are seen in the corresponding spectrum. A feature at ~610 cm^{-1} has also been ascribed to $CoAl_2O_4$ [43]. A weak band at ~715 cm^{-1} shows the existence of a small amount of dispersed CoO_x on the surface of the IWI sample.

In summary, a much better dispersion of cobalt oxide, in the form of amorphous CoO_x in good interaction with the surface prevails over the crystalline phases in the case of the EDF sample and the Co_3O_4 phase in this sample is consisted from relatively small size crystallites. These findings are in very good agreement with the aforementioned textural characteristics of the samples and the results of their XRD analysis.

The above findings are also corroborated by the XPS results. Fig. 7 shows the XP spectra of the Co2p core level for the catalysts studied. In all spectra a major peak appears at ca. 781.4 eV corresponding to the $Co2p_{3/2}$ photoelectrons. The position of this peak as well as the appearance of the satellite lines in the spectral region is well related to Co being in Co_3O_4, $CoAl_2O_4$ and CoO surface phases [52].

The XPS analysis of the samples allows calculating the percentage cobalt atomic surface concentrations (% $Co_{surf.\ atoms}$). The calculated values are summarized in Table 1. These values

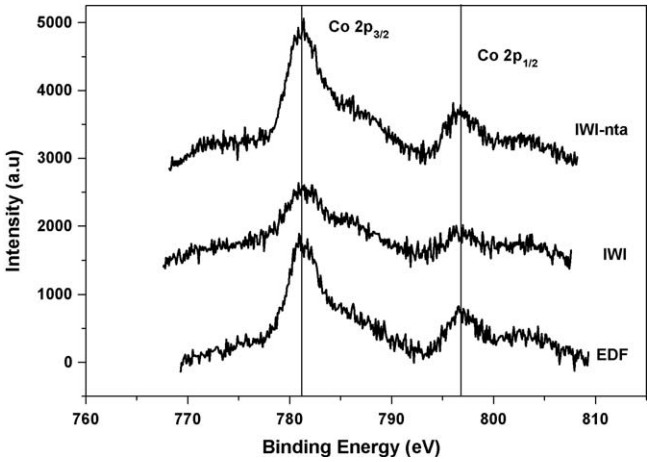

Fig. 7. X-ray photoelectron spectra of the Co2p core level for the CoO_x/Al_2O_3catalysts.

show that the EDF sample exhibited the highest surface concentration of Co. Taking into account that all the studied catalysts have the same bulk concentration of cobalt (21%, w/w) the above results clearly show that, in effect, the EDF catalyst exhibits the highest Co dispersion among the prepared samples.

Temperature-programmed reduction curves of the catalysts studied are presented in Fig. 8. An inspection of these curves reveals that all the samples were irreducible at temperatures lower than 400 °C. This explains why we have not observed any change in the Raman spectra of the samples after H_2 treatment at 300 °C.

The very low hydrogen consumption observed over the EDF catalyst indicates *a very strong interaction between the cobalt phase and the support surface in this sample*. The latter is in very good agreement with the fact that this sample has the highest Co dispersion. On the other hand, the very high hydrogen consumption observed over the IWI-nta sample probably shows that the addition of nitrilotriacetic acid as chelating ligand upon Co deposition prohibits an extended formation of the almost irreducible $CoAl_2O_4$ which is in agreement with the Raman results.

4. Closing remarks

The joint use of different characterization techniques allows demonstrating the influence of the impregnation method on the physicochemical characteristics of the "cobalt oxide/γ-alumina catalysts" calcined at a very high temperature.

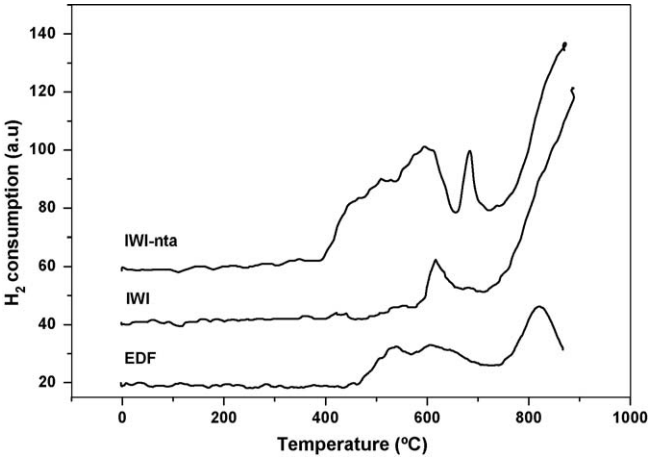

Fig. 8. TPR curves of the CoO_x/Al_2O_3 catalysts.

The EDF methodology, applied under the conditions of the present work, imposes interfacial deposition and results to the formation of an almost bi-dimensional surface precipitate [26,27,29]. Upon calcination, this surface precipitate provides very well-dispersed CoO_x amorphous species strongly interacted with the support surface and thus hardly reducible as well as relatively small Co_3O_4 supported nanocrystals (14.3 nm). The first phase is the predominant one. Therefore, EDF result to catalyst with the highest cobalt surface and specific surface area.

On the other hand, the application of the conventional IWI imposes bulk (solution) precipitation and thus induces relatively large supported crystallites [26,29]. Upon calcination the supported phase provides mainly relatively large supported Co_3O_4 nanocrystals (19.8 nm) and $CoAl_2O_4$ as well. The formation of the relatively large nanocrystals and the insertion of cobalt inside the γ-alumina lattice to form $CoAl_2O_4$ may be responsible for the lowest cobalt surface obtained in this catalyst.

The presence of the nitrilotriacetic acid in the impregnating solution induces the exchange of the water ligands of the Co(II) aqua complex present in the cobalt nitrate solution with organic ligands and thus the bulk precipitation of an organo-metallic complex [26]. The more bulky organic ligands decrease the cobalt-support interactions [26]. Thus, upon calcination of the IWI-nta sample the insertion of cobalt inside the γ-alumina lattice and the formation of $CoAl_2O_4$ are inhibited. This may be responsible for the relatively higher cobalt surface obtained with respect to that achieved in the IWI sample though the size of the Co_3O_4 nanocrystals is larger in the IWI-nta sample (25.8 nm).

Two types of reactions take place over the catalysts studied and the alumina support: methanation of CO and complete oxidation of the CO, CH_4 and H_2. The first type predominates in the temperature range 250–700 °C whereas the second at temperatures higher than 750 °C. At relatively high reaction temperatures all catalysts exhibited almost the same activity for oxidation reactions. In contrast, at low reaction temperatures the EDF catalyst proved to be more active for the CH_4 production as well as for the oxidation of H_2 and CO. This behaviour may be attributed to the favourable physicochemical characteristics of this catalyst.

Acknowledgments

Funding of this work is gratefully acknowledged from the European Commission under the 6th framework programme (SES6-CT-2004-502782).

References

[1] A. Faur Ghenciu, Curr. Opin. Solid State Mater. Sci. 6 (2002) 389.
[2] R. Farrauto, S. Hwang, L. Shore, W. Ruettinger, J. Lampert, T. Giroux, Y. Liu, O. Ilinich, Annu. Rev. Mater. Res. 33 (2003) 1.
[3] R. Burch, P.K. Loader, Appl. Catal. B 5 (1994) 149.
[4] R.M. Siewert, P.J. Mitchell, European Patent 0,468,556 A1, 1991.
[5] L.F. Liotta, G. Di Carlo, G. Pantaleo, G. Deganello, E. Merlone Borla, M. Pidria, Catal. Commun. 8 (2007) 299.
[6] B. Stasinska, W. Gac, T. Ioannides, A. Machocki, J. Nat. Gas Chem. 16 (2007) 342.
[7] J.A.C. Ruiz, M.A. Fraga, H.O. Pastore, Appl. Catal. B-Environ. 76 (2007) 115.
[8] T. Osaki, K. Nagashima, K. Watari, K. Tajiri, Catal. Lett. 119 (2007) 134.
[9] X.H. Wang, Y. Guo, G.Z. Lu, Y. Hu, L.Z. Jiang, Y.L. Guo, Z.G. Zhang, Catal. Today 126 (2007) 369.
[10] K. Persson, L.D. Pfefferle, W. Schwartz, A. Ersson, S.G. Jaras, Appl. Catal. B-Environ. 74 (2007) 242.
[11] S. Cimino, M.P. Casaletto, L. Lisi, G. Russo, Appl. Catal. A-Gen. 327 (2007) 238.
[12] G. Lapisardi, P. Gelin, A. Kaddouri, E. Garbowski, S. Da Costa, Top. Catal. 42–43 (2007) 461.
[13] H. Yoshida, T. Nakajima, Y. Yazawa, T. Hattori, Appl. Catal. B-Environ. 71 (2007) 70.
[14] L.F. Liotta, G. Di Carlo, G. Pantaleo, G. Deganello, Catal. Commun. 6 (2005) 329.
[15] L.M. Shi, W. Chu, F.F. Qu, S.H. Lou, Catal. Lett. 113 (2007) 59.
[16] S. Kwon, M. Fan, T.D. Wheelock, Environ. Eng. Sci. 24 (2007) 1065.
[17] M.A. Pakulska, C.M. Grgicak, J.B. Giorgi, Appl. Catal. A-Gen. 332 (2007) 124.
[18] J. Cheng, H.L. Wang, Z.P. Hao, S.B. Wang, Catal. Commun. 9 (2008) 690.
[19] K.S. Hui, C.Y.H. Chao, C.W. Kwong, M.P. Wan, Combust. Flame 153 (2008) 119.
[20] O. M'Ramadj, B. Zhang, D. Li, X.Y. Wang, G.Z. Lu, J. Nat. Gas Chem. 16 (2007) 258.
[21] R.J. Farrauto, C.H. Bartholomew, In Fundamentals of Industrial Catalytic Processes, Blackie Academic and Professional, Chapman & Hall, London, 1997.
[22] L.F. Liotta, G. Di Carlo, G. Pantaleo, G. Deganello, Appl. Catal. B-Environ. 70 (2007) 314.
[23] F.E. Trigueiro, C.M. Ferreira, J.C. Volta, W.A. Gonzalez, P.G.P. de Oliveria, Catal. Today 118 (2006) 425.
[24] U. Zavyalova, P. Scholz, B. Ondruschka, Appl. Catal. A-Gen. 323 (2007) 226.
[25] K. Bourikas, Ch. Kordulis, J. Vakros, A. Lycourghiotis, Adv. Colloid Interf. Sci. 110 (3) (2004) 97.
[26] Th. Ataloglou, J. Vakros, K. Bourikas, Ch. Fountzoula, Ch. Kordulis, A. Lycourghiotis, Appl. Catal. B 57 (4) (2005) 299.
[27] Th. Ataloglou, Ch. Fountzoula, K. Bourikas, J. Vakros, A. Lycourghiotis, Ch. Kordulis, Appl. Catal. A 288 (1–2) (2005) 1.
[28] A. Sarellas, D. Niakolas, K. Bourikas, J. Vakros, Ch. Kordulis, J. Colloid Interf. Sci. 295 (1) (2006) 165.
[29] K. Bourikas, Ch. Kordulis, A. Lycourghiotis, Catal. Rev. Sci. Eng. 48 (4) (2006) 363.
[30] K. Bourikas, J. Vakros, Ch. Fountzoula, Ch. Kordulis, A. Lycourghiotis, Catal. Today 128 (3–4) (2007) 138.
[31] K. Inamura, K. Uchikawa, S. Matsuda, Y. Akai, Appl. Surf. Sci. 121 (1997) 468.
[32] Ch. Papadopoulou, L. Karakonstantis, H.K. Matralis, Ch. Kordulis, A. Lycourghiotis, Bull. Soc. Chim. Belg. 105 (1996) 247.
[33] I. Georgiadou, Ch. Papadopoulou, H.K. Matralis, G.A. Voyiatzis, A. Lycourghiotis, Ch. Kordulis, J. Phys. Chem. B 102 (1998) 8459.
[34] Ch. Kordulis, A.A. Lappas, Ch. Fountzoula, K. Drakaki, A. Lycourghiotis, I.A. Vasalos, Appl. Catal. A 209 (2001) 85.
[35] A. Lycourghiotis, Ch. Kordulis, K. Bourikas, Encyclopedia of Surface and Colloid Science, Marcel Dekker, Inc., 2002, p. 1366.
[36] J. Vakros, K. Bourikas, Ch. Kordulis, A. Lycourghiotis, J. Phys. Chem. B 107 (2003) 1804.
[37] E.B. Samdell, Colorimetric Determination of Traces of Metals, Interscience, New York, 1950, p. 274.
[38] J. Due-Hansen, S. Boghosian, A. Kustov, P. Fristrup, G. Tsilomelekis, K. Stahl, C. Hviid Christensen, R. Fehrmann, J. Catal. 251 (2007) 459.
[39] C.D. Wagner, L.E. Davis, M.V. Zeller, A.J. Taylor, R.H. Raymond, L.H. Gale, Surf. Interf. Anal. 3 (1981) 211.
[40] N. Spanos, H.K. Matralis, Ch. Kordulis, A. Lycourghiotis, J. Catal. 136 (1992) 432.
[41] J.L. Lemaitre, in: F. Delannay (Ed.), Characterization of Heterogeneous Catalysts, Marcel Decker Inc., New York and Basel, 1984 (Chapter 2).
[42] Y. Zhang, H. Xiong, K. Liew, J. Li, J. Mol. Catal. A: Chem. 237 (2005) 172.
[43] B. Jongsomjit, J. Panpranot, J.G. Goodwin Jr., J. Catal. 204 (2001) 98.
[44] H.K. Matralis, Ch. Papadopoulou, A. Lycourghiotis, Appl. Catal. A 116 (1994) 221.
[45] J. Vakros, Ch. Kordulis, A. Lycourghiotis, Langmuir 18 (2002) 417.
[46] D. Nicholls, Complexes and First-Row Transition Elements, MacMillan Press Ltd., London, 1974, pp. 64–6, 92–7.
[47] A.B.P. Lever, Inorganic Electronic Spectroscopy, 2nd ed., Elsevier, Amsterdam, 1984, pp. 480–505, 736–61, 816–21.
[48] Y. Brik, M. Kacimi, M. Ziyad, F. Bozon-Verduraz, J. Catal. 202 (2001) 118.
[49] V.G. Hadjiev, M.N. Iliev, I.V. Vergilov, J. Phys. C: Solid State Phys. 21 (1988) L199.
[50] D. Gallant, M. Pezolet, S. Simard, J. Phys. Chem. B 110 (2006) 6871.
[51] X.X. Gao, C.J. Huang, N.W. Zhang, J.H. Li, W.Z. Weng, H.L. Wan, Catal. Today 131 (2008) 211.
[52] Z. Zsoldos, L. Guczi, J. Phys. Chem. 96 (1992) 9393.